ISSN 1674-1056
http://cpb.iphy.ac.cn
http://iopscience.iop.org/cpb
中国物理 B
Chinese Physics
中国物理 Chinese Physics B

Mechanisms of atmospheric neutron-induced single event upsets in nanometric SOI and bulk SRAM devices based on experiment-verified simulation tool

Zhi-Feng Lei(雷志锋), Zhan-Gang Zhang(张战刚), Yun-Fei En(恩云飞), Yun Huang(黄云)
Citation: Chin. Phys. B . 2018, 27(6): 066105. **doi:** 10.1088/1674-1056/27/6/066105

Journal homepage: http://cpb.iphy.ac.cn; http://iopscience.iop.org/cpb

What follows is a list of articles you may be interested in

Ab-initio investigation of $AGeO_3$ (*A*=Ca, Sr) compounds via Tran–Blaha-modified Becke–Johnson exchange potential

Rasul Bakhsh Behram, M A Iqbal, Muhammad Rashid, M Atif Sattar, Asif Mahmood, Shahid M Ramay
Chin. Phys. B . 2017, 26(11): 116103. **doi:** 10.1088/1674-1056/26/11/116103

Theoretical prediction of new C-Si alloys in *C*2/*m*-20 structure

Xiangyang Xu(徐向阳), Changchun Chai(柴常春), Qingyang Fan(樊庆扬), Yintang Yang(杨银堂)
Chin. Phys. B . 2017, 26(4): 046101. **doi:** 10.1088/1674-1056/26/4/046101

Comparative study on beryllium and magnesium as a co-doping element for ZnO:N

Yu-Quan Su(苏宇泉), Ming-Ming Chen(陈明明), Long-Xing Su(苏龙兴), Yuan Zhu(祝渊), Zi-Kang Tang(汤子康)
Chin. Phys. B . 2016, 25(6): 066106. **doi:** 10.1088/1674-1056/25/6/066106

Bandgap narrowing in the layered oxysulfide semiconductor $Ba_3Fe_2O_5Cu_2S_2$: Role of FeO_2 layer

Han Zhang(张韩), Shifeng Jin(金士锋), Liwei Guo(郭丽伟), Shijie Shen(申士杰), Zhiping Lin(林志萍), Xiaolong Chen(陈小龙)
Chin. Phys. B . 2016, 25(2): 026101. **doi:** 10.1088/1674-1056/25/2/026101

Theoretical investigation of sulfur defects on structural, electronic, and elastic properties of ZnSe semiconductor

Muhammad Zafar, Shabbir Ahmed, M. Shakil, M. A. Choudhary, K. Mahmood
Chin. Phys. B . 2015, 24(7): 076106. **doi:** 10.1088/1674-1056/24/7/076106

Non-monotonic dependence of current upon i-width in silicon p–i–n diodes

Zheng-Peng Pang(庞正鹏), Xin Wang(王欣), Jian Chen(陈健), Pan Yang(杨盼), Yang Zhang(张洋), Yong-Hui Tian(田永辉), and Jian-Hong Yang(杨建红)†

Institute of Microelectronics, School of Physical Science and Technology, Lanzhou University, Lanzhou 730000, *China*

(Received 11 September 2017; revised manuscript received 23 January 2018; published online 10 May 2018)

Silicon p–i–n diodes with different i-region widths are fabricated and tested. It is found that the current shows the non-monotonic behavior as a function of i-region width at a bias voltage of 1.0 V. In this paper, an analytical model is presented to explain the non-monotonic behavior, which mainly takes into account the diffusion current and recombination current contributing to the total current. The calculation results indicate that the concentration ratio of p-region to n-region plays a crucial role in the non-monotonic behavior, and the carrier lifetime also has a great influence on this abnormal phenomenon.

Keywords: semiconductor, junction diodes, transport properties

PACS: 61.82.Fk, 85.30.Kk, 91.60.Tn **DOI:** 10.1088/1674-1056/27/6/066106

1. Introduction

The p–i–n structures have been widely used in photodetectors,[1–3] power devices,[4] and sensors of fast neutrons,[5] temperature,[6] etc. In addition, the core components of the reconfigurable electro-optical logic circuits are achieved by the p–i–n structures.[7] Recently, a large magnetoresistance was observed with p–i–n diodes.[8] In these structures, the i-layer thickness plays a significant role in device performance. Thus it is essential to study the effect of i-layer thickness on the *I*–*V* characteristics.

The forward *I*–*V* characteristics of p–i–n diodes have been analyzed theoretically by many researchers under reasonable assumptions. Nilsson[9] and Spenke[10] dealt with the *I*–*V* characteristics of a hypothetical symmetrical structure, in which the mobility of electrons was assumed to be equal to that of the holes, and the saturation current of electrons equals that of holes. Howard studied the *I*–*V* characteristics at high forward current densities, in which the recombination current was ignored.[11] Within the limits of Hall's approximation, the diffusion current was ignored.[12] In these studies, either diffusion or recombination current was neglected to study the *I*–*V* characteristics as a function of i-region width. In fact, both the diffusion and recombination occur in the p–i–n diode and contribute to the current transport. Herlet[13] used the asymmetrical structure to study the *I*–*V* characteristics and took into account the diffusion and recombination current, but it is rather complicated to solve the *I*–*V* characteristics equation. In this paper, the *I*–*V* characteristics of the p–i–n junction will be solved using a simple analytical model, and the dependence of non-monotonic behavior of the current on the i-region width will also be studied within the narrow base p–i–n structure.

2. Methods and results

Samples of p–i–n diodes are prepared on SOI substrate by using the standard complementary metal–oxide–semiconductor (CMOS) technology. The silicon-on-insulator (SOI) substrate has a 2-μm BOX layer and a 220-nm Si layer. All samples each have an area of 100 μm ×60 μm, and the i-region widths are intentionally designed ranging from 1 μm–5 μm. Boron implantations are performed with dose I (5.0×10^{13} atom/cm^2, 40 keV) for four samples, and dose II (6.0×10^{13} atom/cm^2, 40 keV) for the other five, the doping concentrations are 5.0×10^{16} cm^{-3} and 6.0×10^{16} cm^{-3} respectively. Phosphorus implantations are performed (45 keV, 8.0×10^{13} atom/cm^2) for all samples, the doping concentration is 8.0×10^{16} cm^{-3}, and the i-region is intrinsic layer. Ohmic contacts are prepared using metals Al/TiN.

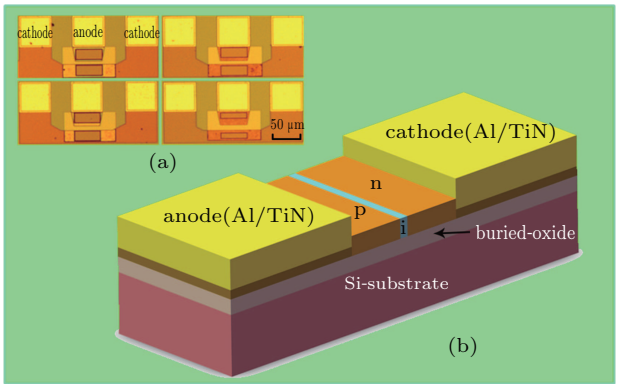


Fig. 1. (color online) (a) Optical micrograph of the samples with different i-widths, and (b) geometric construction schematic diagram of p–i–n diode.

Figure 1(a) shows the optical micrographs of the samples with w = 1, 2, 3, 4 μm from top to bottom and from left to

†Corresponding author. E-mail: yangjh@lzu.edu.cn

© 2018 Chinese Physical Society and IOP Publishing Ltd

right, the micrographs are taken by an Olympus BX51. Figure 1(b) shows the structure of the device.

The *I*–*V* characteristics of the prepared samples are measured by a Keithley 4200. Figures 2(a) and 2(b) show the *I*–*V* curves with the different i-region widths. It can be seen that the sample with i-region width $w = 3$ μm exhibits the largest current no matter what the doping is, while $w = 1$, 2, and 4 μm, the current is smaller than when $w = 3$ μm at the same voltage ($V > 0$). It indicates the current of the p–i–n diode does not always decrease with the increasing of the i-region width at the same voltage ($V > 0$), but increases in some ranges and decreases in other ranges. We call this phenomenon the non-monotonic behavior. Figures 2(c) and 2(d) show each current as a function of i-region width at a bias voltage of 1.0 V for dose I and dose II respectively. The curves are preferable to reveal the non-monotonic behaviors.

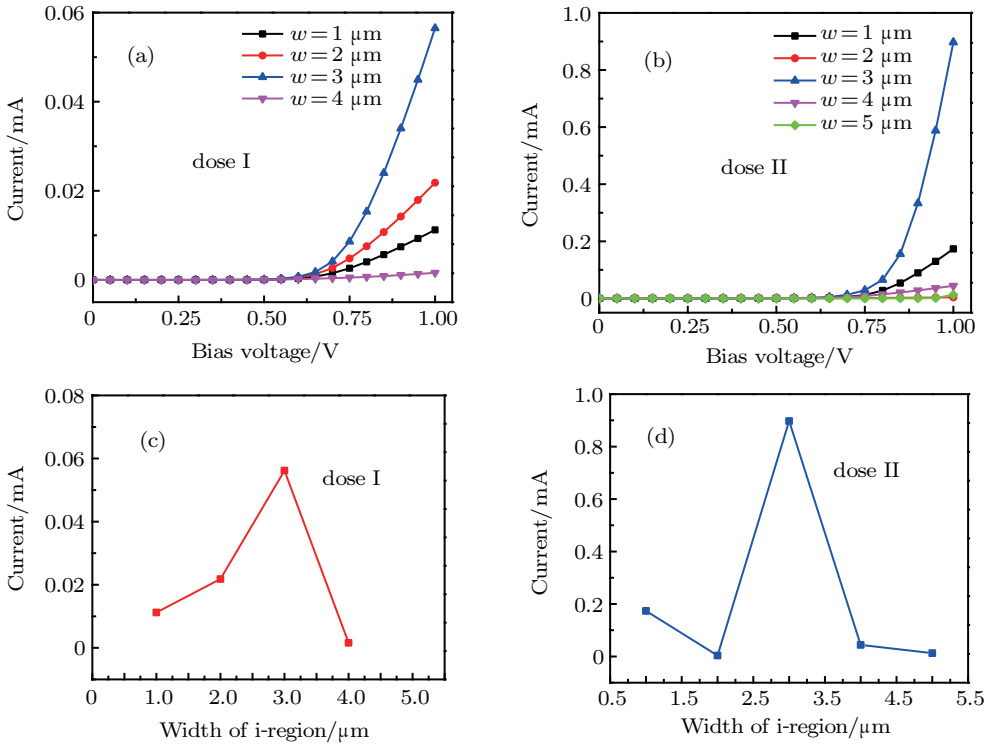


Fig. 2. (color online) [(a) and (b)] Measured *I*–*V* characteristics for dose I and dose II, respectively. [(c) and (d)] Current as a function of i-region width at a bias voltage of 1.0 V for dose I and dose II respectively.

3. Discussion

For the abnormal phenomenon, an analytical model of the current transport is set up to analyze the experimental results. In order to simplify our analysis, we make two appropriate assumptions. Firstly, assuming that neither traps nor impurities were introduced in the production process, so there is no trap-charge that participates in the carrier transportation. Secondly, both p-region and n-region are heavily doped and the i-region is intrinsic, therefore the widths of the space charge region in the p-region and n-region are too narrow to be neglected. Approximately, we assume that the i-region is depleting and the voltage mainly drops in the i-region: there is no voltage drop in the neutral zones in the p-region and n-region.

Figure 3 shows the p–i–n diode schematic diagram of the longitudinal summary mode. The boundary between p-region and i-region is the origin of the coordinate, where x_1 and x_2 are the width of the space charge region between p-region and i-region, respectively, and w is the boundary between i-region and n-region. The spacings between w_1 and w, and w_2 and w are the space charge regions in the i-region and n-region respectively. As the space-charge zones are very narrow in the p-region and n-region, we may substitute $-x_1 \approx 0$ and $w_2 \approx w$ into the equation. V_1 and V_2 are the junction voltages of the p/i-region and n/i-region, respectively, V_i is the voltage drops in the i-region.

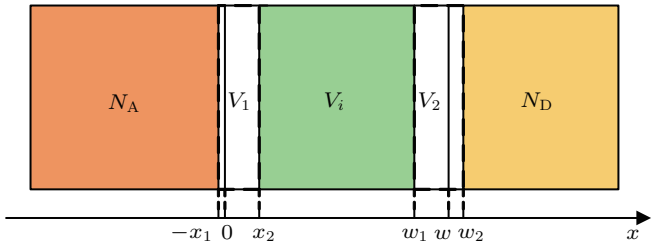


Fig. 3. (color online) Pattern diagram of p–i–n diode. The doping concentrations of p- and n-layers are N_A and N_D, respectively. $x = 0$ and $x = w$ are the doping boundaries.

Our interest lies in the injected carrier distribution in the i-region. It should be noted that the two-type carriers share the same distribution profile in the i-region to keep the quasi-neutrality of this region $p(x) = n(x)$.[9–11] With the aid of the

coordinate system in Fig. 3, the hole concentration $p(x)$ in the i-region can be expressed as

$$p(x) = c_1 \mathrm{e}^{x/L} + c_2 \mathrm{e}^{-x/L}, \tag{1}$$

where

$$c_1 = \frac{1 - s\mathrm{e}^{-w/L}}{\mathrm{e}^{w/L} - \mathrm{e}^{-w/L}} p_{(x=w)},$$

$$c_2 = \frac{s\mathrm{e}^{w/L} - 1}{\mathrm{e}^{w/L} - \mathrm{e}^{-w/L}} p_{(x=w)}, \tag{2}$$

$$p_{(x=w)} = p_{\mathrm{n}}(\mathrm{e}^{V_2/V_{\mathrm{T}}} - 1) \approx p_{\mathrm{n}} \mathrm{e}^{V_2/V_{\mathrm{T}}} \tag{3}$$

with $L = \sqrt{D\tau}$ being the diffusion length, D the diffusion coefficient, τ the lifetime, and $V_{\mathrm{T}} = kT/q$ the thermoelectric potential. Parameter s is the symmetry constant that gives $p(x=0) = sp(x=w)$ and can be reduced to $s = N_{\mathrm{A}}/N_{\mathrm{D}}$ as a good approximation.[13,14] By using $p(x) = n(x)$, the electron concentration in the i-region can be obtained.

According to the Shockley diode model,[15] we think that hole injection current, electron injection current, and recombination current compose the total current. The hole injection current is the diffusion current at the n/i interface, and the electron injection current is the diffusion current at the p/i interface. By calculation, the three current components are obtained as follows:[10,13]

$$\boldsymbol{J}_{\mathrm{n}}(x=0) = \frac{qD}{L}(c_1 - c_2), \tag{4}$$

$$\boldsymbol{J}_{\mathrm{p}}(x=w) = \frac{qD}{L}(c_2 \mathrm{e}^{-w/L} - c_1 \mathrm{e}^{w/L}), \tag{5}$$

$$\boldsymbol{J}_{\mathrm{r}} = \frac{qL}{\tau}\int_0^w p(x)\,\mathrm{d}x = \frac{qL}{\tau}(c_1 \mathrm{e}^{w/L} - c_1 + c_2 - c_2 \mathrm{e}^{-w/L}). \tag{6}$$

Consequently, the net current density of the p–i–n junction is obtained as the sum of the above current densities:

$$\boldsymbol{J} = \boldsymbol{J}_{\mathrm{n}}(x=0) + \boldsymbol{J}_{\mathrm{p}}(x=w) + J_{\mathrm{r}}. \tag{7}$$

The inhomogeneous distribution of injected non-equilibrium carriers forms an electric field in the i-region. Therefore, the voltage V_i can be obtained from the integration of electric field $E(x)$ over the i-region as follows:

$$V_{\mathrm{i}} = \int_0^w E(x)\,\mathrm{d}x = \int_0^w \left(\frac{J}{q(\mu_{\mathrm{n}} + \mu_{\mathrm{p}})p(x)} - V_{\mathrm{T}} \frac{\mu_{\mathrm{n}} - \mu_{\mathrm{p}}}{\mu_{\mathrm{n}} + \mu_{\mathrm{p}}} \frac{\mathrm{d}p(x)}{\mathrm{d}x} \frac{1}{p(x)} \right) \mathrm{d}x. \tag{8}$$

According to the Boltzmann expression and $p(x=0) = sp(x=w)$, V_1 and V_2 can be given by the applied voltage and s.

$$V_1 = \frac{V - V_{\mathrm{i}}}{2} + \frac{V_{\mathrm{T}} \ln(s)}{2}, \quad V_2 = \frac{V - V_{\mathrm{i}}}{2} - \frac{V_{\mathrm{T}} \ln(s)}{2}, \tag{9}$$

With these equations, the total current density can be solved at any required applied voltage by a computer. The parameters used for the calculation are shown in Table 1.

Table 1. Parameters used for calculation.

Symbol	Quantity	Value
D/cm^2·s^{-1}	ambipolar diffusion constant	18.3
N_{D}/cm^{-3}	doping concentration of n-layer	8×10^{16}
n_{i}/cm^{-3}	intrinsic carrier concentration	1.5×10^{10}
N_{I}/cm^{-3}	doping concentration of i-layer	1×10^{13}
μ_{n}/cm^2·s^{-1}·V^{-1}	electron mobility of i-layer	1350
μ_{p}/cm^2·s^{-1}·V^{-1}	hole mobility of i-layer	480
τ/s	carrier lifetime of i-layer	10^{-8}
q/C	elementary charge	1.6×10^{-19}
L/μm	ambipolar diffusion length	13.5

Figure 4(a) shows the simulated curves of the current as a function of w with different values s ($N_{\mathrm{D}} = 8\times10^{16}$ cm^{-3}) at a fixed bias of 0.8 V. From this figure, we can see that there are different variation trends with different s values. When $s = 1.00$ and $s = 0.875$, the simulated results are in good agreement with our experimental results; when $s < 0.875$, the curves show monotonic behavior. Thus the abnormal phenomenon is relevant to the factor s, and the value s is determined by the ratio of the doping concentration of the p-region to that of the n-region, and means the distribution level of the injection carriers in the i-region, indicating that the non-monotonic behavior is intrinsically linked to the injection carriers. When $N_{\mathrm{D}} = 8\times10^{16}$ cm^{-3}, we find that the behavior occurs at $N_{\mathrm{A}} = 7\times10^{16}$ cm^{-3} $\sim 8\times10^{16}$ cm^{-3} from the simulation results.

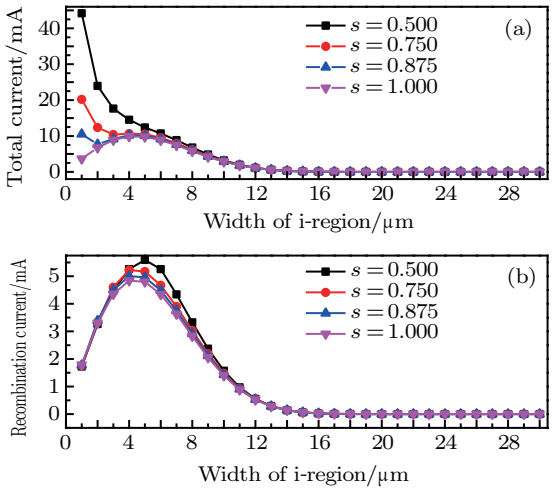


Fig. 4. (color online) Plots of total (a) and recombination (b) currents versus i-layer thickness with different s values and $N_{\mathrm{D}} = 8\times10^{16}$ cm^{-3} at $V_{\mathrm{bias}} = 0.8$ V.

In addition, we calculate the recombination current (Fig. 4(b)). We find that no matter what the factor s is, the recombination current first increases and then decreases with w increasing, while the non-monotonic behavior of the total current is related to s, indicating the injection current plays a leading role in a tiny i-region width for the behavior. When $w > 14$ μm, the total current and recombination current are tiny and maintained, this is because all of the injecting electrons and holes almost occur as recombination events in the i-region, so the recombination current dominates the total current.

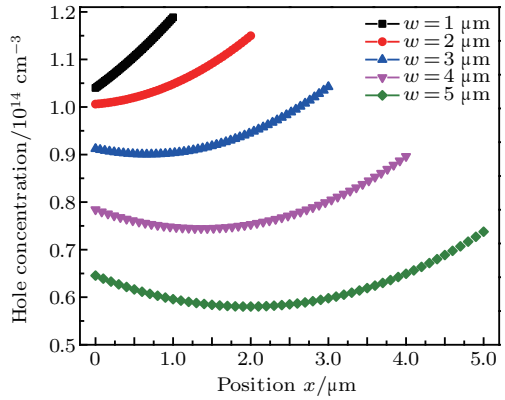


Fig. 5. (color online) Plots of concentration distribution $p(x)$ versus position in the intrinsic region of p–i–n junction with $\tau = 1 \times 10^{-8}$ s and $s = 0.875$.

The hole concentration distribution $p(x)$ is shown in Fig. 5. We can see that although the hole concentration decreases with w increasing, the sum of concentration gradients at $x = 0$ and $x = w$ show the non-monotonic behavior with w increasing. The concentration gradient at the boundary means the size of the electron injection current and hole injection current, respectively, so the injection current is non-monotonic with w increasing. In this paper, we assume that the rate of recombination has a linear relationship with carrier concentration, while the rate of recombination can be expressed as $R = -\gamma_1 n - \gamma_2 n^2 - \gamma_3 n^3 \cdots$; $(p = n)$ according to Ref. [9], γ_1, γ_2, and γ_3 are Shockley–Reid–Hall (SRH), band-to-band, and Auger recombination coefficients. For silicon, we can neglect the second-order term (Ref. [9]), and the third-order recombination dominates when the carrier concentration is higher than 10^{18} cm^{-3}. The concentration of injection carriers is smaller than 10^{18} cm^{-3}, so the rate of recombination can be expressed as $R = -\gamma_1 n$. When w is relatively small, the injection current dominates the total current, so the total current increases with w increasing, when w increases and is greater than a critical width, the recombination current dominates the total current, so the total current decreases with w increasing.

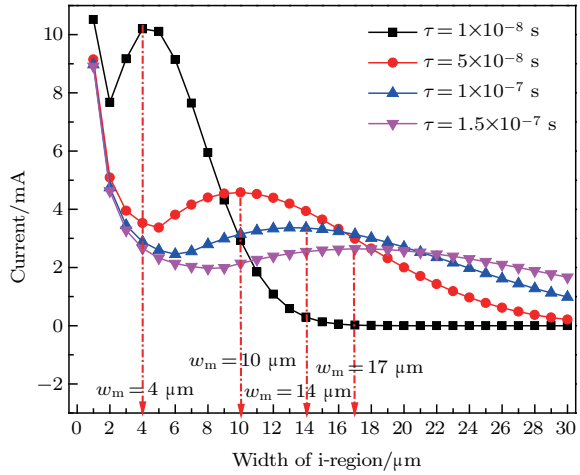


Fig. 6. (color online) Plots of current versus i-region width for different carrier lifetimes ($s = 0.875$).

As discussed before, the injected carriers present recombination in the i-region, and the recombination current plays a crucial role in abnormal phenomenon. Thus, we study the relationship between the current and the carrier lifetime. As shown in Fig. 6, the carrier lifetime has a great influence on the non-monotonic behavior, which makes the maximum value shifted from 4 μm to 17 μm when τ changes from 1×10^{-8} s to 1.5×10^{-7} s, and the critical width (W_m) increases with carrier lifetime increasing.

When the carrier lifetime increases, less carriers present recombination and most carriers are injected into the boundary of the i-region. As a result, the injection current dominates the total current. With the increase of the width, it is difficult to inject the carriers into the boundary, so the recombination current regains its dominant function. Consequently, the critical width becomes bigger when the lifetime increases.

4. Conclusions

In the present work, the I–V characteristics of the p–i–n devices with different i-region widths have been investigated experimentally and theoretically. It is found that the current shows the non-monotonic behavior as a function of i-region width at a fixed voltage, which is a meaningful finding. In theoretical analysis, both the diffusion current and the recombination current are taken into account to refine the I–V characteristic of the p–i–n junction. For the non-monotonic behavior, the injection current plays an important role in the tiny i-region width, while the recombination current is dominated for the case of the large i-region width. On the other hand, the concentration ratio between p-region and n-region and carrier lifetime prove to be related to the experimental abnormal phenomenon. The concentration ratio has an influence on the variation trend of the curves, and the lifetime determines the critical width.

References

[1] Xue H Y, Xue C L, Cheng B W, Yu Y D and Wang Q W 2010 *IEEE Electron Dev. Lett.* **31** 701
[2] Zheng J, Wang S Y, Liu Z, Cong H, Xue C L, Li C B, Zuo Y H, Cheng B W and Wang Q M 2016 *Appl. Phys. Lett.* **108** 033503
[3] Mathews J, Roucka R, Xie J Q, Yu S Q, Menéndez J and Kouvetakis J 2009 *Appl. Phys. Lett.* **95** 133506
[4] Kaji N, Niwa H, Suda J and Kimoto T 2015 *IEEE Trans. Electron Dev.* **62** 374
[5] Rosenfeld A B, Yudelev M, Lerch M L F, Cornelius I, Griffin P, Perevertailo V L, Anokhin I E, Zinets O S, Khivrich V I, Pinkovskaya M, Alexiev D and Reinhard M 2003 *IEEE Trans. Nucl. Sci.* **50** 2367
[6] Rao S, Pangallo G and Corte F G D 2016 *IEEE Trans. Electron Dev.* **63** 414
[7] Qiu C Y, Ye X, Soref R, Yang L and Xu Q F 2012 *Opt. Lett.* **37** 3942
[8] Yang D Z, Wang F C, Ren Y, Zuo Y L, Peng Y, Zhou S M and Xue D S 2013 *Adv. Funct. Mater.* **23** 2918
[9] Nilsson N G 1973 *Solid-State Electron.* **16** 681
[10] Spenke E 1968 *Solid-State Electron.* **11** 1119
[11] Howard N R and Johnson G W 1965 *Solid-State Electron.* **8** 275
[12] Hall R N 1952 *Proc. IRE* **40** 1512
[13] Herlet A 1968 *Solid-State Electron.* **11** 717
[14] Dutton R W and Whittier R J 1969 *IEEE Trans. Electron Dev.* **16** 458
[15] Shockley W B 1949 *Bell System Tech. J.* **28** 435